



HAL
open science

Burma Terrane part of the Trans-Tethyan arc during collision with India according to palaeomagnetic data

Jan Westerweel, Pierrick Roperch, Alexis Licht, Guillaume Dupont-Nivet, Zaw Win, Fernando Poblete, Gilles Ruffet, Hnin Hnin Swe, Myat Kai Thi, Day Wa Aung

► **To cite this version:**

Jan Westerweel, Pierrick Roperch, Alexis Licht, Guillaume Dupont-Nivet, Zaw Win, et al.. Burma Terrane part of the Trans-Tethyan arc during collision with India according to palaeomagnetic data. Nature Geoscience, 2019, 12 (10), pp.863-868. 10.1038/s41561-019-0443-2 . insu-02283010

HAL Id: insu-02283010

<https://insu.hal.science/insu-02283010>

Submitted on 16 Nov 2020

HAL is a multi-disciplinary open access archive for the deposit and dissemination of scientific research documents, whether they are published or not. The documents may come from teaching and research institutions in France or abroad, or from public or private research centers.

L'archive ouverte pluridisciplinaire **HAL**, est destinée au dépôt et à la diffusion de documents scientifiques de niveau recherche, publiés ou non, émanant des établissements d'enseignement et de recherche français ou étrangers, des laboratoires publics ou privés.

Burma Terrane part of the Trans-Tethyan arc during collision with India according to palaeomagnetic data

Jan Westerweel^{1*}, Pierrick Roperch¹, Alexis Licht², Guillaume Dupont-Nivet^{1,3}, Zaw Win⁴, Fernando Poblete^{1,5}, Gilles Ruffet¹, Hnin Hnin Swe⁶, Myat Kai Thi⁶ and Day Wa Aung⁶

Convergence between the Indian and Asian plates has reshaped large parts of Asia, changing regional climate and biodiversity, yet geodynamic models fundamentally diverge on how convergence was accommodated since the India–Asia collision. Here we report palaeomagnetic data from the Burma Terrane, which is at the eastern edge of the collision zone and is famous for its Cretaceous amber biota, to better determine the evolution of the India–Asia collision. The Burma Terrane was part of a Trans-Tethyan island arc and stood at a near-equatorial southern latitude at ~95 Ma, suggesting island endemism for the Burmese amber biota. The Burma Terrane underwent significant clockwise rotation between ~80 and 50 Ma, causing its subduction margin to become hyper-oblique. Subsequently, it was translated northward on the Indian Plate by an exceptional distance of at least 2,000 km along a dextral strike-slip fault system in the east. Our reconstructions are only compatible with geodynamic models involving an initial collision of India with a near-equatorial Trans-Tethyan subduction system at ~60 Ma, followed by a later collision with the Asian margin.

The Himalayan–Tibetan orogen, resulting from terrane amalgamation including the India–Asia collision, is commonly considered to be a natural laboratory for continent–continent collisional systems, yet the palaeogeography of the India–Asia collision remains a controversial issue^{1–5} with widely different competing geodynamic models. For decades, a simple model prevailed proposing that the Indian plate moved northward until collision of Greater India with the Asian margin in the Eocene^{1,6}. However, updated information supporting a Palaeocene (~58 Ma (ref. 7)) collision age, alongside tectonic constraints, put the Indian continent at a near-equatorial latitude at that time, thousands of kilometres away from the southern Asian margin^{3–6,8–13}. A Palaeocene collision could still be compatible with this first model by assuming an Asian margin at a low latitude (~10° N (ref. 6)), but this position is invalidated by palaeomagnetic data¹⁴. Alternatively, an extra-large continental Greater India⁴ could explain a Palaeocene collision age. However, this scenario would require an unrealistic continental subduction of India⁴ and a major shortening of the Asian margin, which can only be partly solved by lateral extrusion of the Indochina Blocks away from the collision zone^{3,6,9–11}, but remains much higher than accounted for by structural data¹⁵. Two new models have recently been proposed that assume the following: (1) the existence of an oceanic basin between India and Greater India that could have easily subducted after an initial collision of Greater India with Asia at 58 Ma until a second collision of India with Asia in the Miocene^{5,12} or (2) the existence of a Trans-Tethyan subduction system with which the Indian continent would initially collide at ~60 to 50 Ma before jointly colliding with Asia later in the Palaeogene^{2,8,13,16,17}. Such a double subduction zone may also better account for the rapid India–Asia convergence before the final collision⁸.

The palaeogeographic evolution of the Burma Terrane (BT, also named the West Burma Block) at the eastern edge of the collision zone differs in these geodynamic scenarios and therefore offers a way to determine the most realistic model (Fig. 1). In the continental Greater India models^{3,6,9,10}, the BT is located at a relatively high latitude during the Palaeogene, next to the Lhasa Terrane as part of a linear and approximately east–west-oriented Asian margin. From this position, the BT is extruded towards its present-day location. The volcanic Wuntho–Popa Arc of the BT was interpreted as the eastward continuation of the Gangdese magmatic arc required in these models; however, the arc is currently oriented approximately north to south (Fig. 2). Therefore, these models necessitate significant post-collisional clockwise rotation for the BT. In the oceanic Greater India models^{5,12}, the Asian margin is less deformed during the collision and the BT experiences little post-collisional rotation. Finally, the position of the BT is less constrained in the Trans-Tethyan subduction models. Most reconstructions involving double subduction show the BT north of Sumatra^{13,17}, but it could have also been part of the Incertus Arc, the island arc of the Trans-Tethyan subduction system¹⁷, which would potentially allow a more southern latitude for the BT during the earlier periods of collision^{2,8,13,16,17}.

Presently, the palaeogeographic evolution of the BT is virtually undocumented, despite being of critical importance for biodiversity studies; the fossil amber from the BT harbours one of the most diverse and largest known records of Cretaceous biota^{18,19}. Furthermore, the palaeogeography of the BT is important for palaeoenvironmental studies investigating Asian monsoonal history^{20,21}. This study aims to fill this gap and solve these controversies by providing necessary constraints on the motion of the BT using new palaeomagnetic and ⁴⁰Ar/³⁹Ar age data.

¹Géosciences Rennes, CNRS and Université de Rennes 1, Rennes, France. ²Department of Earth and Space Sciences, University of Washington, Seattle, WA, USA. ³Department of Earth Sciences, Potsdam University, Potsdam, Germany. ⁴Department of Geology, University of Shwebo, Shwebo, Myanmar.

⁵Instituto de Ciencias de la Ingeniería, Universidad de O'Higgins, Rancagua, Chile. ⁶Department of Geology, University of Yangon, Yangon, Myanmar.

*e-mail: jan.westerweel@univ-rennes1.fr

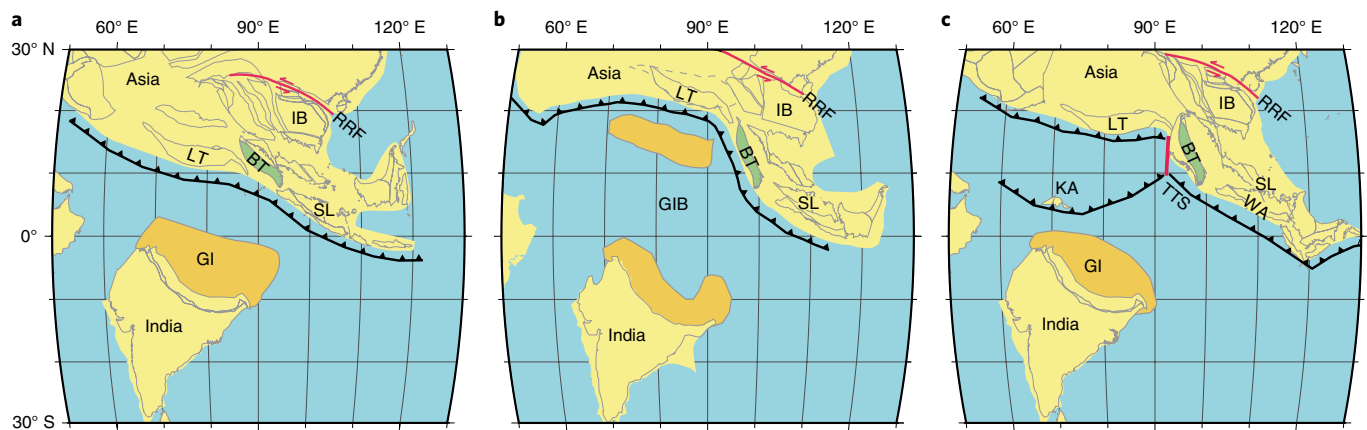


Fig. 1 | Alternative plate reconstructions of India-Asia palaeogeography at 60 Ma. **a**, Reconstruction with a nearly linear subduction zone and significant extrusion of Indochina Blocks^{6,9}. **b**, Reconstruction with a Greater India Basin⁵. **c**, Reconstruction with a second Trans-Tethyan subduction zone¹³. (See also Methods.) GI(B), Greater India (Basin); IB, Indochina Blocks; KA, Kohistan Arc; LT, Lhasa Terrane; RRF, Red River Fault (accommodating Indochina extrusion); SL, Sundaland Block; TTS, Trans-Tethyan subduction system; WA, Woyla Arc. Figure constructed using Gplates software and adapted dataset from ref. ⁵¹, Wiley.

Geology of the Burma Terrane

The present-day BT geodynamic setting is characterized by hyper-oblique subduction of the Indian plate below the Burmese margin in the west and by the large-scale, active dextral strike-slip Sagaing Fault in the east, resulting in a northward transcurrent motion of the terrane²². The western boundary of the BT is delineated by either another strike-slip fault (the Kabaw Fault) or the Naga Hills–Kalemyo–Andaman Ophiolite (herein called the Western Belt Ophiolite) in the Indo-Burman Ranges (IBR)^{23–26}. The IBR basement has been interpreted as either (1) a separate tectonic block accreted to the BT either in the Early Cretaceous²⁷ or in the Late Cretaceous to Palaeogene^{16,26} or (2) an accretionary-type setting without block collision^{21,28,29}. East of the BT, there is a complex succession of metamorphic rocks (the Mogok–Mandalay–Mergui Belt, or MMMB) that forms the boundary of the BT with the Shan Plateau (Sibumasu Block) alongside the Sagaing Fault and the Jade Belt Ophiolite²⁶. The complete dextral displacement along this fault system has been estimated to be between 400 and 1,100 km (refs. ^{30–32}). Before the development of the Sagaing Fault, there is evidence for dextral deformation along the Shan Scarp, directly east of the Sagaing Fault^{33,34}, although the tectonic regime of the Sibumasu Block was predominantly sinistral³⁵. Another example of earlier dextral deformation is the late Oligocene West Andaman Fault to the south³⁴.

The oldest exposed rocks of the BT are the low-grade metamorphic Triassic Shwedaung and Pane Chaung Formations, as well as the higher-grade Kanpetlet Schist. Both a late Mesozoic Gondwanan³⁶ or Cathaysian³⁷ origin has been suggested for the Pane Chaung Formation on the basis of detrital zircon uranium-lead (U–Pb) age data. The Burmese margin formed as an Andean-type setting during the Cretaceous, as evidenced by Andean-type magmatic activity in the Wuntho–Popa Arc that today crops out in the middle of a wide belt of forearc and back-arc basins, which developed contemporaneously in Central Myanmar (Fig. 2)^{21,27,38}. Published U–Pb data indicate an early Late Cretaceous main phase of magmatism from 110 to 85 Ma, followed by a subordinate stage from 40 to 70 Ma (refs. ^{24,27,39,40}). Our new 97 to 87 Ma ⁴⁰Ar/³⁹Ar dates in the Kanza Chaung Batholith, the main unit of the northern Wuntho–Popa Arc (Fig. 2, Supplementary Dataset 1), confirm this major magmatic phase. The Western Belt Ophiolite was probably emplaced during that time as well^{21,27,28,38,41}. The Wuntho–Popa Arc has been correlated with the similar Gangdese Arc (Lhasa Terrane)^{24,27}. The

correlation of (1) the Gangdese Arc with the Wuntho–Popa Arc and (2) the Western Belt Ophiolite with the Tibetan Yarlung–Tsangpo Suture Zone^{24,25} are key arguments for the BT to have been located at a latitude similar to the present day and for its position to have been next to the Lhasa Terrane before the India–Asia collision. However, the Mawgyi Andesite, which is most likely part of the Wuntho–Popa Arc (see Supplementary Information), has been correlated with the intra-oceanic mid-Cretaceous Woyla Arc (Sumatra)^{17,23,30} as part of the Incertus Arc (Fig. 1)¹⁷. Subsequent studies continue the Incertus arc farther west by incorporating the Kohistan Arc (Pakistan)^{8,13}.

Palaeomagnetic study

A palaeomagnetic pole was obtained from a homoclinal sedimentary sequence in the late Eocene (~38 Ma from a dated tuff layer²¹) shallow-marine Yaw Formation in the Chindwin Basin, the northernmost forearc basin of Myanmar (Fig. 2). Furthermore, an early Late Cretaceous pole was obtained from five localities (Pinlebu, Shinpa, Banmauk, Kawlin and Kyaung Le) in the Wuntho Range, which is the predominantly Cretaceous (~110 to 85 Ma (refs. ^{24,40})) northern segment of the Wuntho–Popa Arc, where the volcanic and sedimentary rocks of the Kondan Chaung Group are intruded by igneous (I-type) intrusions (Kanza Chaung Batholith) and andesitic stocks (Mawgyi Andesite). Detailed information on the geology, palaeomagnetic analysis and ⁴⁰Ar/³⁹Ar dating is provided in the Methods, Supplementary Information and Supplementary Datasets 1–3.

The late Eocene samples are from mudstones and siderite beds with primary detrital or early-diagenetic magnetizations, mostly carried by magnetite. They yield well-defined antipodal normal and reverse-polarity directions in coherent magnetozones, resulting in a mean with a north-oriented declination and shallow positive inclination in tectonic coordinates (Fig. 3a, Supplementary Dataset 1). This mean palaeomagnetic direction corresponds to a negligible rotation ($4.6 \pm 3.5^\circ$) compared to stable Eurasia⁴² and a near-equatorial latitude of $2.4 \pm 1.5^\circ$ N. A slightly higher, but not significantly different $4.1 \pm 2.3^\circ$ N palaeolatitude is obtained after inclination-shallowing corrections (see Supplementary Information). This result is corroborated by similarly low inclinations obtained from the siderite beds devoid of shallowing, and it is in general agreement with the low impact of inclination shallowing in sedimentary rocks at low latitudes when compared to middle to high latitudes⁴³.

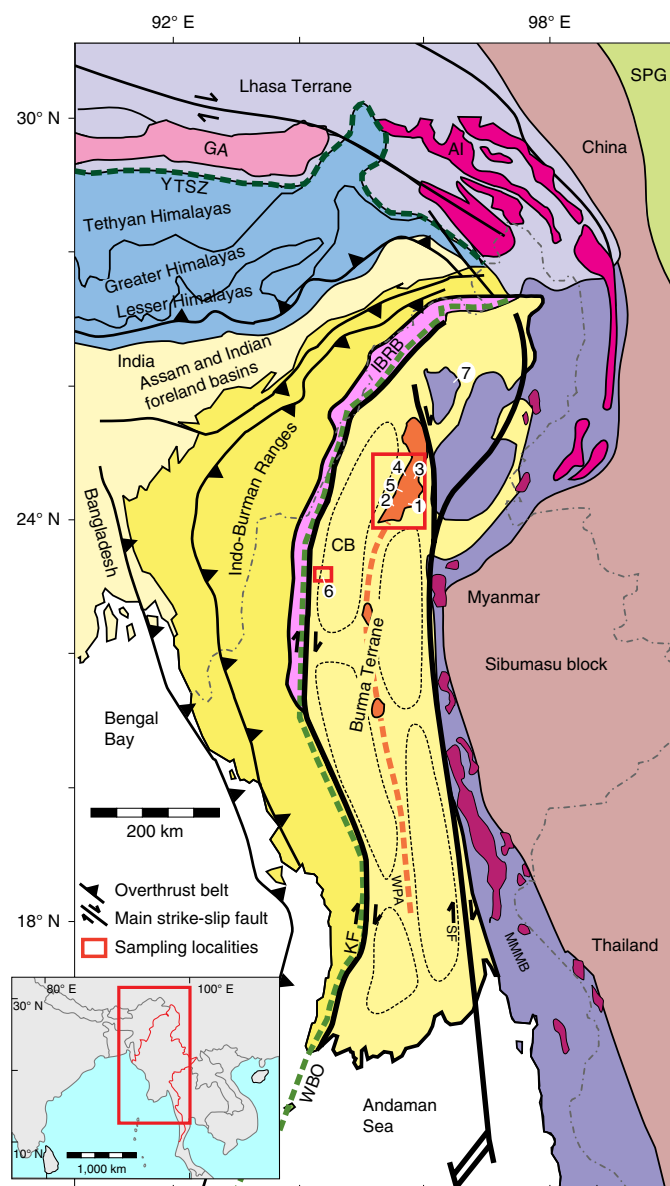


Fig. 2 | Generalized geologic map of Myanmar and neighbouring countries. Localities: 1, Kawlin; 2, Pinlebu; 3, Banmauk; 4, Kyaung Le; 5, Shinpa; 6, Kalewa; 7, Burmese amber^{18,19}. AI, Cretaceous to Palaeogene Asian intrusive rocks; CB, Chindwin Basin; GA, Cretaceous Gangdese Arc; IBRB, Indo-Burman Ranges basement; KF, Kabaw Fault; MMBB, Mogok-Mandalay-Mergui Belt (including Jurassic Eastern Belt Ophiolites and Jade Belt Ophiolite); SF, Sagaing Fault; SPG, Songpan Ganze and Yangtze complexes; WBO, Cretaceous Western Belt Ophiolite; WPA, Wuntho-Popa Arc; YTSZ, Yarlung-Tsangpo Suture Zone. Dashed black lines, boundaries of Central Myanmar Basins. Figure adapted from ref. ²¹, GSA.

In early Late Cretaceous rocks from the Wuntho Range, reliable directions were obtained from samples of (1) the Kanza Chaung Batholith (Pinlebu, Shinpa and Banmauk sites) with characteristic remanent magnetizations (ChRM) carried by magnetite and (2) the Kondan Chaung Group (Kawlin and Kyaung Le sites), both of which were homogeneously magnetized during emplacement of the batholith as shown by our petrologic observations and $^{40}\text{Ar}/^{39}\text{Ar}$ dates (see Supplementary Information). The blocking temperatures of the ChRMs are similar to the closure temperatures in $^{40}\text{Ar}/^{39}\text{Ar}$ dating, suggesting the age of magnetization of

the Wuntho Range rocks to be ~ 97 to 87 Ma, in accordance with the existing Wuntho-Popa Arc U-Pb data^{24,40}. A systematic trend to east-directed declinations and horizontal to slightly negative inclinations can be inferred from our data (Supplementary Dataset 1), despite significant differences in rock types and magnetic properties. Tilting is recorded by rocks of the Kondan Chaung Group, but occurred before the intrusion of the batholith in most cases. No field evidence for significant tilting of the Kanza Chaung Batholith was observed, which is in agreement with our anisotropy of magnetic susceptibility data (see Supplementary Information). If we omit data from brecciated and non-homogeneously hydrothermally altered sites from the Mawgyi Andesite (Kawlin) and the westernmost sites from the Kondan Chaung Group (Kyaung Le), which were slightly tilted after acquiring their magnetization, we obtain a similar but better defined overall final mean direction for the Wuntho Range from 16 sites (Fig. 3b, Supplementary Dataset 1). The mean corresponds to a slightly southern hemisphere palaeolatitude of $5.0 \pm 4.7^\circ\text{S}$ for the BT in the early Late Cretaceous and a significant clockwise rotation ($60.4 \pm 8.7^\circ$) with respect to the expected direction from stable Eurasia⁴². Although we cannot discard a component of local rotation associated with dextral shear, the systematic rotation values and the regionally coherent north-south trends of the batholith and main tectonic structures suggest that the mean declination better reflects a complete rotation of the BT. The different palaeomagnetic results for the Chindwin Basin and the Wuntho Range imply that most rotation of the BT occurred between the early Late Cretaceous and late Eocene with ~ 800 km of northward motion (Fig. 3c). The near-equatorial early Late Cretaceous to late Eocene palaeolatitudes implied by our data are in stark contrast to previous studies, usually placing the BT close to its present-day location since the early Cenozoic^{17,24,26,27,34}, and these data therefore have major tectonic implications.

Tectonic implications

The southern hemisphere shallow latitude at ~ 95 Ma for the Wuntho-Popa Arc was distant from the southern Asian margin and Indochina and is therefore best explained as having been formed above a near-equatorial Trans-Tethyan subduction system, as part of the Incertus Arc, with northward-subducting Neo-Tethyan oceanic lithosphere (Fig. 4)⁸. This interpretation is further supported by the development of the Burmese margin as an Andean-type setting around that time (Late Cretaceous) and coeval emplacement of the Western Belt Ophiolite^{21,24,27,28,38,40,41}. The Trans-Tethyan subduction system could have been partly intra-oceanic, possibly incorporating the Kohistan Arc, which also formed at a near-equatorial latitude^{8,44}. Because the Indonesian Woyla Arc is interpreted as having been already accreted at ~ 90 Ma (refs. ^{17,23}), we reconstructed a transform fault east of the BT, accommodating an earlier collision between the Woyla Arc and the Sundaland Block.

The major clockwise rotation of the BT between 95 and 40 Ma (Fig. 4) may have been linked either to the accretion of the BT to the margin of the southern Sibumasu and northern Sundaland Blocks or to the collision of India with the Trans-Tethyan subduction system. In support of the latter possibility is that in most models with Trans-Tethyan subduction^{8,13,16}, decreasing convergence rates between India and Asia at ~ 60 to 50 Ma are associated with a collision of the (Greater) Indian continent with the arc. At the eastern end of this collision, the thin Indian continental crust may thus have interacted with the BT, causing its clockwise rotation⁴⁵. However, the exact timing and mechanism of this rotation needs to be refined with future research.

Since the late Eocene (~ 38 Ma (ref. ²¹)), our results indicate a significant $\sim 2,000$ km northward motion, coeval with the motion of India (Fig. 4), during a period when Indochina was extruded towards the southeast^{46–49}. The results suggest that the northward motion of the BT was coupled with the Indian Plate. Our palaeo-

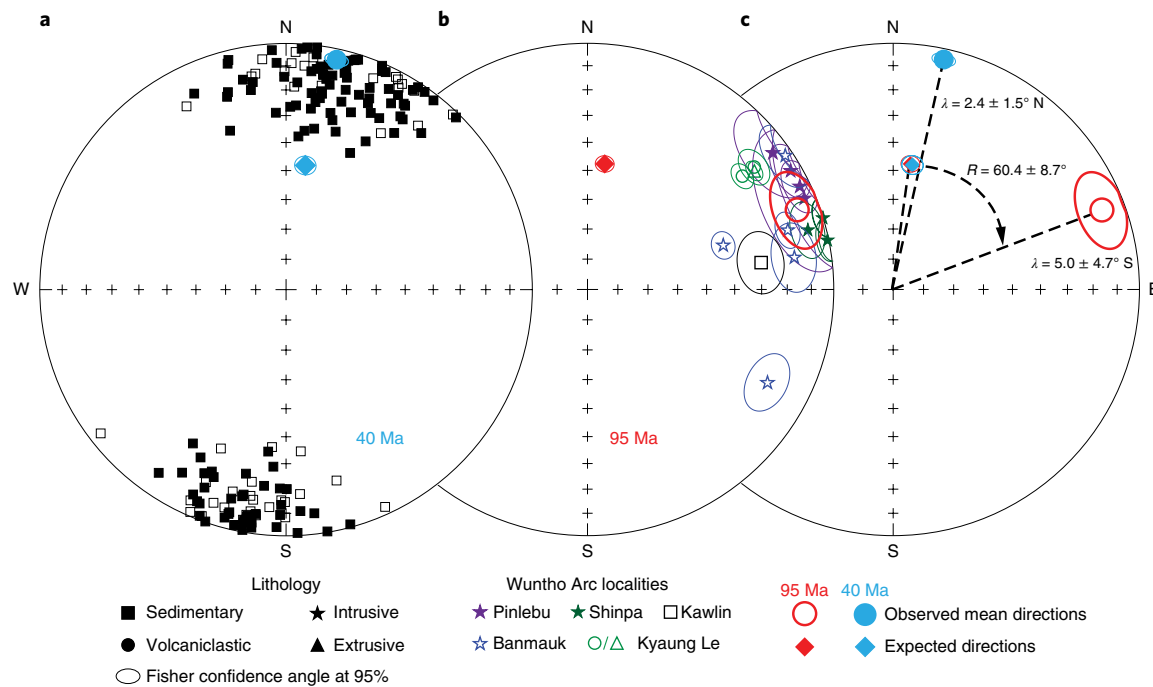


Fig. 3 | Equal-area projections of interpretable palaeomagnetic results. a, Tilt-corrected characteristic directions (squares) of samples from late Eocene sediments from Kalewa and mean direction (blue). **b,** Early Late Cretaceous Wuntho Range site means with 95% confidence angles in in-situ coordinates, coloured by locality: Pinlebu (purple), Shinpa (dark green), Banmauk (blue), Kawlin (black) and Kyaung Le (green); mean direction shown in red. **c,** Early Late Cretaceous to late Eocene (red and blue circles) final mean directions compared with the stable Eurasia apparent polar wander path in the early Late Cretaceous to late Eocene (red and blue diamonds)⁴². λ , palaeolatitudes calculated from the mean inclinations and R , rotation magnitude are indicated with 95% confidence angles. Open and closed symbols denote negative and positive inclinations, respectively.

magnetic data indicate that the Burmese subduction margin was already oriented approximately north-south in the late Eocene, such that subduction of the Indian Plate beneath the BT was already hyper-oblique. This hyper-obliquity provided a mechanism for the full partitioning of the Burmese subduction margin relative to Indochina and its coupling with the Indian motion; it is also consistent with the inferred onset of pull-apart subsidence in the Chindwin Basin²¹ and a significant decrease in Wuntho-Popa Arc magmatism at ~38 Ma (refs. ^{27,40}). Furthermore, the coeval motion of the BT and India suggests that dextral wrenching within the IBR was not important until the Neogene.

Hence, the northward motion of the BT since the late Eocene required a major dextral strike-slip system east of the BT. However, the ~2,000 km of northward motion indicated by our palaeomagnetic data is much more than the ~400 km of motion estimated along the active dextral Sagaing Fault at the eastern margin of the BT³¹. Furthermore, the age of the Sagaing Fault (Quaternary, Neogene or older) remains debated^{30–32}. A precursor dextral strike-slip system is thus required by our data, the pathway and location of which remains enigmatic and has probably been obscured by posterior activity of the Sagaing Fault and the opening of the Andaman Sea. The potential remnants of this precursor strike-slip system are an early segment of the Sagaing Fault^{33,34} or the Oligocene West Andaman Fault³⁴. The latter could have effectively separated the BT to its west from the developing Eastern Andaman Basins and the predominantly sinistral tectonic regime of the Sibumasu Block to its east as the BT moved northward and passed west of these features (Fig. 4)^{32,34,35}. This separation potentially explains why the late Eocene sedimentary infill of the Central Myanmar Basins was predominantly derived from an Andean-type arc, probably the Wuntho-Popa Arc, with an increasing contribution of older metamorphic detritus in the Oligocene

and Miocene²¹ as the BT moved closer to the Sibumasu Block and the eastern Himalayan syntaxis.

Additionally, the low late Eocene palaeolatitude for the BT demonstrates that an India-BT collision next to the Lhasa Terrane² was impossible. Instead, the near-equatorial latitude of the BT provided the space and free border for the lateral extrusion of the Tengshong and Baoshan Blocks, which rotated clockwise by ~40° to 70° (refs. ^{47,48}) and, to a minor extent, the Indochina Block, which rotated ~15° to 20°, all of which occurred mainly during the Oligocene and Miocene. The Oligocene and Miocene included periods of major sinistral deformation along the main shear zones separating these blocks^{46,49}. The northward motion and later emplacement without rotation of the BT also accounts for the striking difference between the linear north-south orientation of the Sagaing Fault and, directly to the west, the curvilinear sinistral faults (Gaoligong, Wanding, Nanting) associated with the clockwise rotations in the Tengshong and Baoshan Blocks.

Beyond geodynamics, our results suggest that the BT was isolated as part of the Incertus Arc at the time of deposition of the prolific Cretaceous Burmese fossil ambers, which raises questions about the potential endemic character of the amber biota and their connection with species from India, Gondwana and southeastern Asia^{18,19}. From a palaeoenvironmental perspective, our near-equatorial palaeolatitudes for the BT are surprising, considering the evidence for a strongly seasonal climate in Myanmar in the Eocene²⁰. Strong seasonality at Eocene equatorial latitudes in southeastern Asia is corroborated by independent evidence from palaeoclimatic data from Java⁵⁰. Palaeomagnetic and palaeoenvironmental data can only be reconciled with a massive seasonal migration of the Intertropical Convergence Zone over southeastern Asia, confirming well-marked South Asian monsoons during the Eocene²⁰; however, future climate models incorporating our new reconstructions will be needed to verify the migration.

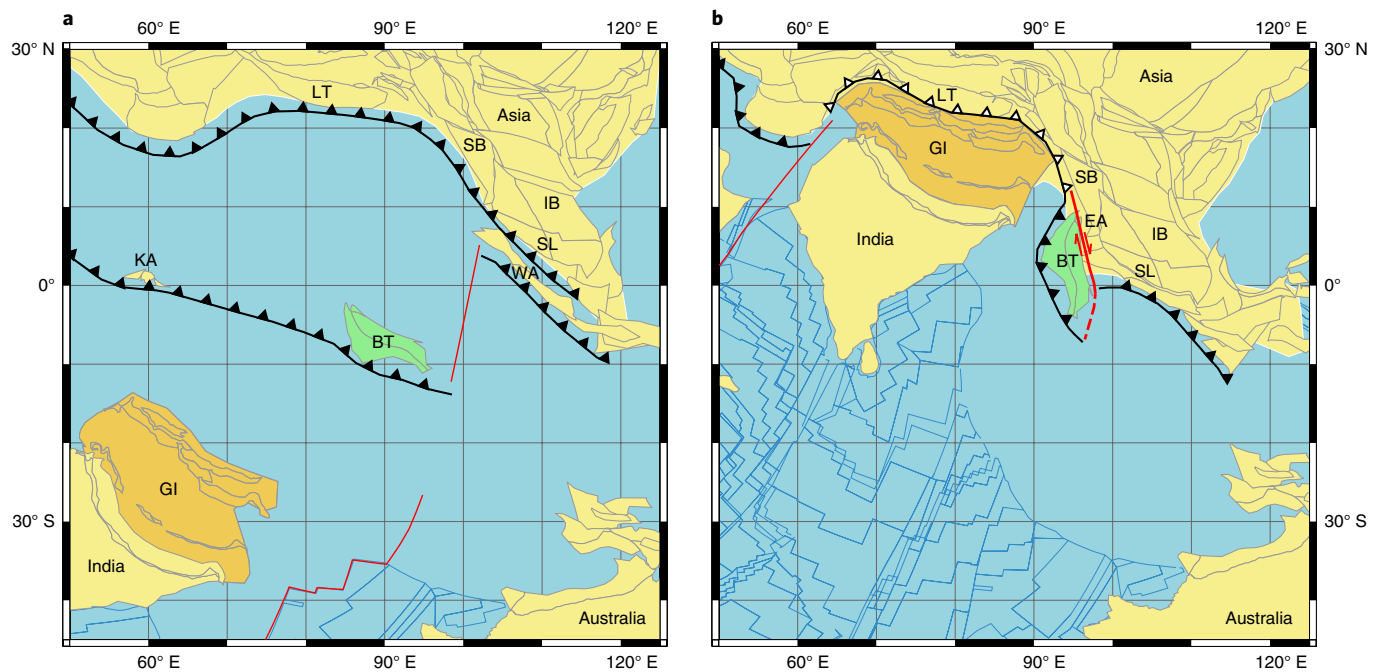


Fig. 4 | Reconstructions of the Burma Terrane and Asia. a, 95 Ma. b, 40 Ma. (See also Methods). EA, Eastern Andaman Basins; GI, Greater India; SB, Sibumasu Block. Thin blue lines, seafloor magnetic isochrons on present-day oceanic crust; red lines, postulated oceanic ridges and transform faults. Figure constructed using Gplates software and adapted dataset from ref. ⁵¹, Wiley.

The foremost conclusion from our palaeomagnetic results is that they are incompatible with both continental and oceanic Greater India models and are best interpreted in a geodynamic framework with a Trans-Tethyan subduction system accommodating India–Asia convergence. As part of this system, the BT was a segment of the Incertus Arc when Neo-Tethyan subduction began in the Late Cretaceous. In the period that included the early Palaeogene collision of India with the Trans-Tethyan subduction system, the BT rotated $\sim 60^\circ$ clockwise and then moved northward at least 2,000 km since ~ 38 Ma as part of the Indian Plate along a dextral strike-slip system until it reached its present-day position. Hence, our findings provide much-needed evidence to settle a longstanding geodynamic debate on the India–Asia collision and the existence of a Trans-Tethyan subduction system. Furthermore, they pave the way to a reinterpretation of regional structural and palaeogeographic data by taking into account the near-equatorial position of the BT during the Late Cretaceous to Eocene as part of this system.

Online content

Any methods, additional references, Nature Research reporting summaries, source data, statements of code and data availability and associated accession codes are available at <https://doi.org/10.1038/s41561-019-0443-2>.

Received: 2 November 2018; Accepted: 2 August 2019;

Published online: 9 September 2019

References

- Molnar, P. & Tapponnier, P. Cenozoic tectonics of Asia: effects of a continental collision: features of recent continental tectonics in Asia can be interpreted as results of the India–Eurasia collision. *Science* **189**, 419–426 (1975).
- Aitchison, J. C., Ali, J. R. & Davis, A. M. When and where did India and Asia collide? *J. Geophys. Res.* **112**, B05423 (2007).
- Replumaz, A., Negredo, A. M., Guillot, S. & Villaseñor, A. Multiple episodes of continental subduction during India/Asia convergence: insight from seismic tomography and tectonic reconstruction. *Tectonophysics* **483**, 125–134 (2010).
- Ingalls, M., Rowley, D. B., Currie, B. & Colman, A. S. Large-scale subduction of continental crust implied by India–Asia mass-balance calculation. *Nat. Geosci.* **9**, 848–853 (2016).
- van Hinsbergen, D. J. J. et al. Reconstructing Greater India: Paleogeographic, kinematic, and geodynamic perspectives. *Tectonophysics* **760**, 69–94 (2018).
- Cogne, J.-P., Besse, J., Chen, Y. & Hankard, F. A new Late Cretaceous to present APWP for Asia and its implications for paleomagnetic shallow inclinations in central Asia and Cenozoic Eurasian plate deformation. *Geophys. J. Int.* **192**, 1000–1024 (2013).
- Hu, X. et al. The timing of India–Asia collision onset – facts, theories, controversies. *Earth Sci. Rev.* **160**, 264–299 (2016).
- Jagoutz, O., Royden, L., Holt, A. F. & Becker, T. W. Anomalous fast convergence of India and Eurasia caused by double subduction. *Nat. Geosci.* **8**, 475–478 (2015).
- Replumaz, A., Guillot, S., Villaseñor, A. & Negredo, A. M. Amount of Asian lithospheric mantle subducted during the India/Asia collision. *Gondwana Res.* **24**, 936–945 (2013).
- Royden, L. H., Burchfiel, B. C. & van der Hilst, R. D. The geological evolution of the Tibetan plateau. *Science* **321**, 1054–1058 (2008).
- Tapponnier, P., Peltzer, G., Le Dain, A. Y., Armijo, R. & Cobbold, P. Propagating extrusion tectonics in Asia: new insights from simple experiments with plasticine. *Geology* **10**, 611–616 (1982).
- van Hinsbergen, D. J. J. et al. Greater India basin hypothesis and a two-stage Cenozoic collision between India and Asia. *Proc. Natl Acad. Sci. USA* **109**, 7659–7664 (2012).
- Zahirovic, S., Seton, M. & Müller, R. D. The Cretaceous and Cenozoic tectonic evolution of southeast Asia. *Solid Earth* **5**, 227–273 (2014).
- Dupont-Nivet, G., Lippert, P. C., Van Hinsbergen, D. J. J., Meijers, M. J. M. & Kapp, P. Palaeolatitude and age of the Indo–Asia collision: palaeomagnetic constraints: palaeolatitude and age of the Indo–Asia collision. *Geophys. J. Int.* **182**, 1189–1198 (2010).
- van Hinsbergen, D. J. J. et al. Restoration of Cenozoic deformation in Asia and the size of Greater India. *Tectonics* **30**, TC5003 (2011).
- Gibbons, A. D., Zahirovic, S., Müller, R. D., Whittaker, J. M. & Yatheesh, V. A tectonic model reconciling evidence for the collisions between India, Eurasia and intra-oceanic arcs of the central-eastern Tethys. *Gondwana Res.* **28**, 451–492 (2015).
- Hall, R. Late Jurassic–Cenozoic reconstructions of the Indonesian region and the Indian Ocean. *Tectonophysics* **570–571**, 1–41 (2012).
- Poinar, G. Jr. Burmese amber: evidence of Gondwanan origin and Cretaceous dispersal. *Hist. Biol.* <https://doi.org/10.1080/08912963.2018.1446531> (2018).

19. Grimaldi, D. A., Engel, M. S. & Nascimbene, P. C. *Fossiliferous Cretaceous Amber from Myanmar (Burma): Its Rediscovery, Biotic Diversity, and Paleontological Significance* American Museum Novitates No. 3361 (American Museum of Natural History, 2002).
20. Licht, A. et al. Asian monsoons in a late Eocene greenhouse world. *Nature* **513**, 501–506 (2014).
21. Licht, A. et al. Paleogene evolution of the Burmese forearc basin and implications for the history of India-Asia convergence. *Geol. Soc. Am. Bull.* **131**, 730–748 (2018).
22. Socquet, A. et al. India and Sunda plates motion and deformation along their boundary in Myanmar determined by GPS. *J. Geophys. Res. Solid Earth* **111**, B05406 (2006).
23. Barber, A. J. & Crow, M. J. Structure of Sumatra and its implications for the tectonic assembly of southeast Asia and the destruction of Paleotethys. *Isl. Arc* **18**, 3–20 (2009).
24. Mitchell, A., Chung, S.-L., Oo, T., Lin, T.-H. & Hung, C.-H. Zircon U–Pb ages in Myanmar: magmatic–metamorphic events and the closure of a neo-Tethys ocean? *J. Asian Earth Sci.* **56**, 1–23 (2012).
25. Liu, C.-Z. et al. Tethyan suturing in southeast Asia: zircon U–Pb and Hf–O isotopic constraints from Myanmar ophiolites. *Geology* **44**, 311–314 (2016).
26. Searle, M. P. et al. Chapter 12 Tectonic and metamorphic evolution of the Mogok metamorphic and Jade Mines belts and ophiolite terranes of Burma (Myanmar). *Geol. Soc. Lond. Mem.* **48**, 261–293 (2017).
27. Zhang, P. et al. Structures, uplift, and magmatism of the western Myanmar arc: constraints to mid-Cretaceous–Paleogene tectonic evolution of the western Myanmar continental margin. *Gondwana Res.* **52**, 18–38 (2017).
28. Fareeduddin, A. & Dilek, Y. Structure and petrology of the Nagaland–Manipur Hill Ophiolitic Mélange zone, NE India: A fossil Tethyan subduction channel at the India–Burma plate boundary. *Episodes* **38**, 298–314 (2015).
29. Zhang, J. et al. Multiple alternating forearc- and backarc-ward migration of magmatism in the Indo–Myanmar orogenic belt since the Jurassic: documentation of the orogenic architecture of eastern Neotethys in SE Asia. *Earth Sci. Rev.* **185**, 704–731 (2018).
30. Mitchell, A. H. G. Cretaceous–Cenozoic tectonic events in the western Myanmar (Burma)–Assam region. *J. Geol. Soc. London* **150**, 1089–1102 (1993).
31. Morley, C. K. Syn-kinematic sedimentation at a releasing splay in the northern Minwun Ranges, Sagaing fault zone, Myanmar: significance for fault timing and displacement. *Basin Res.* **29**, 684–700 (2017).
32. Morley, C. K. & Arboit, F. Dating the onset of motion on the Sagaing Fault: evidence from detrital zircon and titanite U–Pb geochronology from the north Minwun basin, Myanmar. *Geology* **47**, 581–585 (2019).
33. Bertrand, G. & Rangin, C. Tectonics of the western margin of the Shan plateau (central Myanmar): implication for the India–Indochina oblique convergence since the Oligocene. *J. Asian Earth Sci.* **21**, 1139–1157 (2003).
34. Morley, C. K. Chapter 4 Cenozoic rifting, passive margin development and strike-slip faulting in the Andaman Sea: a discussion of established v. new tectonic models. *Geol. Soc. Lond. Mem.* **47**, 27–50 (2017).
35. Morley, C. K. Nested strike-slip duplexes, and other evidence for Late Cretaceous–Palaeogene transpressional tectonics before and during India–Eurasia collision, in Thailand, Myanmar and Malaysia. *J. Geol. Soc. London* **161**, 799–812 (2004).
36. Yao, W. et al. Origin and tectonic evolution of Upper Triassic turbidites in the Indo-Burman ranges, West Myanmar. *Tectonophysics* **721**, 90–105 (2017).
37. Sevastjanova, I. et al. Myanmar and Asia united, Australia left behind long ago. *Gondwana Res.* **32**, 24–40 (2016).
38. Pivnik, D. A. et al. Polyphase deformation in a fore-arc/back-arc basin, Salin subbasin, Myanmar (Burma). *Am. Assoc. Pet. Geol. Bull.* **82**, 1837–1856 (1998).
39. Gardiner, N. J. et al. Contrasting granite metallogeny through the zircon record: a case study from Myanmar. *Sci. Rep.* **7**, 748 (2017).
40. Wang, J.-G., Wu, F.-Y., Tan, X.-C. & Liu, C.-Z. Magmatic evolution of the western Myanmar arc documented by U–Pb and Hf isotopes in detrital zircon. *Tectonophysics* **612–613**, 97–105 (2014).
41. Singh, A. K. et al. Evidence of mid-ocean ridge and shallow subduction forearc magmatism in the Nagaland–Manipur ophiolites, northeast India: constraints from mineralogy and geochemistry of gabbros and associated mafic dykes. *Geochemistry* **76**, 605–620 (2016).
42. Torsvik, T. H. et al. Phanerozoic polar wander, palaeogeography and dynamics. *Earth Sci. Rev.* **114**, 325–368 (2012).
43. Arason, P. & Levi, S. Models of inclination shallowing during sediment compaction. *J. Geophys. Res.* **95**, 4481–4499 (1990).
44. Zaman, H. & Torii, M. Palaeomagnetic study of Cretaceous red beds from the eastern Hindukush Ranges, northern Pakistan: palaeoreconstruction of the Kohistan–Karakoram composite unit before the India–Asia collision. *Geophys. J. Int.* **136**, 719–738 (1999).
45. Rangin, C., Maurin, T. & Masson, F. Combined effects of Eurasia/Sunda oblique convergence and East–Tibetan crustal flow on the active tectonics of Burma. *J. Asian Earth Sci.* **76**, 185–194 (2013).
46. Leloup, P. H., Tapponnier, P., Lacassin, R. & Searle, M. P. Discussion on the role of the Red River shear zone, Yunnan and Vietnam, in the continental extrusion of SE Asia. *J. Geol. Soc. London* **164**, 1253–1260 (2007).
47. Li, S., van Hinsbergen, D. J. J., Deng, C., Advokaat, E. L. & Zhu, R. Paleomagnetic constraints from the Baoshan area on the deformation of the Qiangtang–Sibumasu terrane around the eastern Himalayan syntaxis. *J. Geophys. Res. Solid Earth* **123**, 977–997 (2018).
48. Tong, Y.-B. et al. Internal crustal deformation in the northern part of Shan–Thai block: new evidence from paleomagnetic results of Cretaceous and Paleogene redbeds. *Tectonophysics* **608**, 1138–1158 (2013).
49. Wang, Y. et al. Kinematics and ⁴⁰Ar/³⁹Ar geochronology of the Gaoligong and Chongshan shear systems, western Yunnan, China: implications for early Oligocene tectonic extrusion of SE Asia. *Tectonophysics* **418**, 235–254 (2006).
50. Evans, D., Müller, W., Oron, S. & Renema, W. Eocene seasonality and seawater alkaline earth reconstruction using shallow-dwelling large benthic foraminifera. *Earth Planet. Sci. Lett.* **381**, 104–115 (2013).
51. Müller, R. D. et al. GPlates: building a virtual Earth through deep time. *Geochem. Geophys. Geosyst.* **19**, 2243–2261 (2018).

Acknowledgements

This research was primarily funded by the European Research Council's consolidator grant MAGIC (Monsoons in Asia caused Greenhouse to Icehouse Cooling) no. 649081 to G.D.-N. We thank C. Kissel for the use of the AGM magnetometer at the Laboratoire des Sciences du Climat et de l'Environnement's palaeomagnetic laboratory, France. Furthermore, we thank L. Joanny and F. Gouttefanges for their help with scanning electron microscope data acquisition. We are grateful to P. Cullerier and A. Bernard for their help in the laboratory. We thank E. Advokaat, F. Fluteau, S. Guillot, E. Hallot, C. Rangin, A. Replumaz, M. Searle and D. van Hinsbergen for prolific discussions in the course of this study. Finally, we are grateful to C. Morley, R. Hall and J. Geissman for their constructive comments, which helped to clarify our data presentation and model.

Author contributions

P.R., A.L. and G.D.-N. conceived the project. J.W., P.R., A.L., G.D.-N., Z.W., F.P., H.H.S., M.K.T. and D.W.A. participated in the sampling. J.W. and P.R. performed the palaeomagnetic analysis. G.R. performed the radiometric analysis. J.W., P.R. and E.B. built the GPlates model. J.W., P.R., A.L. and G.D.-N. wrote the manuscript with contributions from other authors.

Competing interests

The authors declare no competing interests.

Additional information

Supplementary information is available for this paper at <https://doi.org/10.1038/s41561-019-0443-2>.

Reprints and permissions information is available at www.nature.com/reprints.

Correspondence and requests for materials should be addressed to J.W.

Publisher's note: Springer Nature remains neutral with regard to jurisdictional claims in published maps and institutional affiliations.

© The Author(s), under exclusive licence to Springer Nature Limited 2019

Methods

Palaeomagnetic sampling. Conventional palaeomagnetic core plug samples were obtained from two localities in the BT in northern Myanmar. Sampling and determining the orientation of the samples were done using standard palaeomagnetic field equipment and procedures with both magnetic and sun compasses. The first locality covers the early Late Cretaceous intrusive, extrusive, volcanoclastic and sedimentary rocks of the Wuntho Range near the towns of Kawlin, Pinlebu, Shinpa, Banmauk and Kyaung Le. The second locality includes the late Eocene sedimentary rocks of the Chindwin forearc basin near the town of Kalewa. A detailed geologic setting, including regional maps, is described in the Supplementary Information.

We sampled 19 sites in intrusive rocks, 13 sites in extrusive rocks and 9 sites in sedimentary rocks of early Late Cretaceous age in the Wuntho Range; most samples were obtained by drilling into recently exposed quarries or rivers, providing fresh samples with almost no weathering. Most samples from the intrusive rocks were obtained around Pinlebu, Shinpa and Banmauk in the western and northern part of the study area. These samples were taken from the regional I-type Kanza Chaung Batholith, which constitutes the main component of the Wuntho Range. Near Kawlin in the southern part of the study area, 11 sites were taken from extrusive rocks of the Mawgyi Andesite Formation. The volcanic rocks were often massive or brecciated; hence, they did not yield clear bedding orientations. Apart from these andesites, two sites were obtained near Kawlin from sandstones of the volcanic-sedimentary Kondan Chaung Group, which was characterized by clearly observable bedding, and one undefined stock. At Kyaung Le in the northernmost part of the study area, all sites were obtained from the Kondan Chaung Group and consisted of nine sedimentary and volcanoclastic rocks, one rhyodacitic rock, and one undefined extrusive rock.

In the Chindwin Basin, 520 samples were collected from the late Eocene shallow-marine Yaw Formation in a continuous homoclinal Cenozoic sedimentary section near Kalewa, as well as from two additional sites. Most of these samples were mudstones and sandstones, and we also collected several samples in siderite-rich carbonate beds intercalated in the mudstones.

Palaeomagnetic analysis. Natural remanent magnetizations were measured on a 2G cryogenic magnetometer hosted in a magnetically shielded room at the University of Rennes 1. Stepwise demagnetization was used to isolate their ChRM components using either (1) thermal demagnetization, with increments of 20° to 50°C up to 680°C or (2) 3-axis alternating field demagnetization, with increments of 2.5 to 10 mT up to 120 mT. During the alternating field demagnetization, the gyromagnetic magnetizations were cancelled by measuring the magnetization after each axis of alternating field demagnetization⁵². Samples with interpretable components were grouped by site after isolating their ChRM using principal component analysis⁵³ and, when necessary, a great-circle approach⁵⁴. Subsequently, mean directions and corresponding statistical parameters were calculated by site and finally by locality using Fisher statistics^{55,56}. Whenever possible, the fold test⁵⁷ was used to investigate whether the magnetization was pre- or post-tectonic in origin. To check whether normal and reverse polarities from the same locality were antiparallel, the classic coordinate bootstrap reversal test was used⁵⁸. Finally, due to the lack of volcanic rocks in the late Eocene sedimentary section, we checked for inclination shallowing in the results from this area by using several approaches, including (1) the classic elongation versus inclination method^{59–61} and (2) an assumption that the sedimentary package consists of uniform rigid particles, which rotate during burial and attending compaction⁶².

In addition to obtaining mean directions, the magnetic properties of the samples were investigated using several methods. After each thermal demagnetization step, the bulk magnetic susceptibility of the samples was measured. To investigate the mineralogy and magnetic properties for a selection of samples, we measured mass-normalized bulk magnetic susceptibility curves with increasing temperature steps up to 580°C on a KLY3-CS3 AGICO Kappabridge, as well as magnetic hysteresis loops on an alternating gradient magnetometer (AGM 2900). To further identify the possible effect of a magnetic fabric on the remanent magnetization for the different rocks, the anisotropy of magnetic susceptibility was determined for most samples on a KLY3S AGICO Kappabridge. In highly anisotropic intrusive igneous rocks, thermal remanent magnetization vectors may be deflected from the direction of the field upon cooling below the Curie point of magnetite, which was the main magnetic carrier in those rocks. However, most of the anisotropy of magnetic susceptibility was probably dictated by multidomain magnetite, yet the magnetic carriers of the remanent magnetization (the finest grained magnetite) may have had a different magnetic fabric. For this reason, we investigated the anisotropy of remanent magnetization in selected samples of intrusive rocks. The thermal remanent magnetization anisotropy correction is common in palaeomagnetism, but we did not attempt this because it requires heating the samples above 580°C (the general natural remanent magnetization unblocking temperature) and alteration is likely to occur after heating to higher temperatures. The anisotropy of isothermal remanent magnetization was performed on selected samples instead. The isothermal remanent magnetization acquisition was done on x_z , $-x_y$, $-y_z$, $-z_x$ at 600 mT, well above the saturation field of magnetite (250 mT). After each measurement, the sample was alternating field demagnetized at 20 mT to remove

the lowest magnetic coercivity fraction. In most cases, 90% of the full isothermal remanent magnetization was randomized at 20 mT.

A detailed description of the various ChRM characteristics, mean calculations, tests and magnetic properties is given by locality in the Supplementary Information. The palaeomagnetic results by site and locality are given in Supplementary Dataset 1 the results from all samples are listed in Supplementary Dataset 2.

Petrology. Polished thin sections were made from selected samples from different lithologies for observation under an optical microscope in transmitted light and reflected light. The samples were then analysed with a scanning electron microscope (JEOL JSM 7100F with Oxford energy dispersive X-ray spectroscopy and electron backscatter diffraction) at the Centre de Microscopie Électronique à Balayage et Microanalyse-ScanMAT platform (University of Rennes 1). Our petrologic observations are described in the Supplementary Information.

⁴⁰Ar/³⁹Ar dating. There are only a few available U-Pb age data available for the Wuntho Range volcanic complex^{24,39}. Therefore, we carried out ⁴⁰Ar/³⁹Ar dating on 14 samples from our palaeomagnetic sites in order to better understand the ages of these rocks and their resulting ChRMs.

The samples were analysed with an ⁴⁰Ar/³⁹Ar laser probe and a Map 215 mass spectrometer. Analyses were performed on millimeter-sized grains of single biotite or amphibole crystals, carefully handpicked under a binocular microscope from crushed rocks. For samples with a fine-grained matrix from which it was not possible to extract biotites or amphiboles, experiments were performed on whole-rock samples.

The irradiation of the samples was performed at the McMaster Nuclear Reactor (Hamilton, Ontario, Canada) in the 8F facility and lasted 66,667 h with a global efficiency (J h⁻¹) of $9.767 \times 10^{-5} \text{ h}^{-1}$. The irradiation standard was sanidine from the Taylor Creek Rhyolite ($28.608 \pm 0.033 \text{ Ma}$ (refs. ^{63–65})).

Apparent age errors were plotted at the 1 σ level and do not include the errors on the ⁴⁰Ar/³⁹Ar_K ratio and age of the monitor and decay constant. Plateau ages were calculated if 70% or more of the ³⁹Ar_K was released in at least three or more contiguous steps where the apparent ages agreed to within 1 σ of the integrated age of the plateau segment. Pseudo-plateau ages can be defined with less than 70% of the ³⁹Ar_K released and in possibly less than three contiguous steps. The errors on the ⁴⁰Ar/³⁹Ar_K ratio and age of the monitor and decay constant are included in the final calculation of the error margins on the pseudo-plateau ages.

The analytical data and parameters used for calculations (for example, isotopic ratios measured on potassium, calcium and chlorine pure salts; mass discrimination; atmospheric argon ratios; J parameter; decay constants) and reference sources are available in Supplementary Dataset 3.

Plate model. For our final geodynamic model, we used the global rotations and continental polygons from the Matthews GPlates model^{51,66} as a template. From this template, we modified the tectonic history of the BT to reflect our palaeomagnetic results. Furthermore, the positions and palaeogeography of Greater India, Indochina, the Kohistan Arc, the Lhasa Terrane, Sumatra and the Woyla Arc were configured to better reflect more recent studies^{8,67,68}. In Fig. 1b, the global reconstruction with the Greater India basin hypothesis is based on a different set of poles of rotations⁵. All plate tectonic reconstructions were made in the combined hotspot (0–70 Ma) and palaeomagnetic (70–250 Ma) reference frame that is also used in the Matthews GPlates model^{66,69}. See Supplementary Information for a detailed discussion on the choice for this reference frame.

Data availability

The authors declare that all data supporting the findings of this study are available within the main article, its Supplementary Information, Supplementary Dataset 1 (palaeomagnetic mean directions), Supplementary Dataset 2 (palaeomagnetic data per sample) and Supplementary Dataset 3 (⁴⁰Ar/³⁹Ar data and parameters).

References

- Roperch, P. & Taylor, G. K. The importance of gyromagnetic remanence in alternating field demagnetization. Some new data and experiments on GRM and RRM. *Geophys. J. Int.* **87**, 949–965 (1986).
- Kirschvink, J. L. The least-squares line and plane and the analysis of palaeomagnetic data. *Geophys. J. Int.* **62**, 699–718 (1980).
- McFadden, P. L. & McElhinny, M. The combined analysis of remagnetisation circles and direct observation in palaeomagnetism. *Earth Planet. Sci. Lett.* **87**, 161–172 (1988).
- Butler, R. F. *Paleomagnetism: Magnetic Domains to Geologic Terranes* (Blackwell Scientific Publications, 1992).
- Fisher, R. Dispersion on a sphere. *Proc. R. Soc. Lond. A* **217**, 295–305 (1953).
- Tauxe, L. & Watson, G. S. The fold test: an eigen analysis approach. *Earth Planet. Sci. Lett.* **122**, 331–341 (1994).
- Tauxe, L. *Essentials of Paleomagnetism* (University of California Press, 2010).

59. King, R. F. The remanent magnetism of artificially deposited sediments. *Geophys. J. Int.* **7**, 115–134 (1955).
60. Tauxe, L. & Kent, D. V. in *Timescales of the Geophysical Field*, Geophysical Monograph Vol. 145 (ed. Channell, J.) 101–116 (American Geophysical Union, 2004).
61. Tauxe, L., Kodama, K. P. & Kent, D. V. Testing corrections for paleomagnetic inclination error in sedimentary rocks: a comparative approach. *Phys. Earth Planet. In.* **169**, 152–165 (2008).
62. Cogné, J.-P. *Contribution à l'Étude Paléomagnétique des Roches Déformées*. Doctorat d'Etat thesis, Université Rennes 1 (1987).
63. Renne, P. R. et al. Intercalibration of standards, absolute ages and uncertainties in $^{40}\text{Ar}/^{39}\text{Ar}$ dating. *Chem. Geol.* **145**, 117–152 (1998).
64. Renne, P. R., Mundil, R., Balco, G., Min, K. & Ludwig, K. R. Joint determination of ^{40}K decay constants and $^{40}\text{Ar}^*/^{40}\text{K}$ for the Fish Canyon sanidine standard, and improved accuracy for $^{40}\text{Ar}/^{39}\text{Ar}$ geochronology. *Geochim. Cosmochim. Acta* **74**, 5349–5367 (2010).
65. Renne, P. R., Balco, G., Ludwig, K. R., Mundil, R. & Min, K. Response to the comment by W.H. Schwarz et al. on “Joint determination of ^{40}K decay constants and $^{40}\text{Ar}^*/^{40}\text{K}$ for the Fish Canyon sanidine standard, and improved accuracy for $^{40}\text{Ar}/^{39}\text{Ar}$ geochronology” by P.R. Renne et al. (2010). *Geochim. Cosmochim. Acta* **75**, 5097–5100 (2011).
66. Matthews, K. J. et al. Global plate boundary evolution and kinematics since the late Paleozoic. *Glob. Planet. Change* **146**, 226–250 (2016).
67. Advokaat, E. L. et al. Cenozoic rotation history of Borneo and Sundaland, SE Asia revealed by paleomagnetism, seismic tomography, and kinematic reconstruction. *Tectonics* **37**, 2486–2512 (2018).
68. Li, S. et al. Paleomagnetic constraints on the Mesozoic-Cenozoic paleolatitudinal and rotational history of Indochina and South China: review and updated kinematic reconstruction. *Earth Sci. Rev.* **171**, 58–77 (2017).
69. Torsvik, T. H., Müller, R. D., Van der Voo, R., Steinberger, B. & Gaina, C. Global plate motion frames: toward a unified model. *Rev. Geophys.* **46**, RG3004 (2008).

Terms and Conditions

Springer Nature journal content, brought to you courtesy of Springer Nature Customer Service Center GmbH (“Springer Nature”).

Springer Nature supports a reasonable amount of sharing of research papers by authors, subscribers and authorised users (“Users”), for small-scale personal, non-commercial use provided that all copyright, trade and service marks and other proprietary notices are maintained. By accessing, sharing, receiving or otherwise using the Springer Nature journal content you agree to these terms of use (“Terms”). For these purposes, Springer Nature considers academic use (by researchers and students) to be non-commercial.

These Terms are supplementary and will apply in addition to any applicable website terms and conditions, a relevant site licence or a personal subscription. These Terms will prevail over any conflict or ambiguity with regards to the relevant terms, a site licence or a personal subscription (to the extent of the conflict or ambiguity only). For Creative Commons-licensed articles, the terms of the Creative Commons license used will apply.

We collect and use personal data to provide access to the Springer Nature journal content. We may also use these personal data internally within ResearchGate and Springer Nature and as agreed share it, in an anonymised way, for purposes of tracking, analysis and reporting. We will not otherwise disclose your personal data outside the ResearchGate or the Springer Nature group of companies unless we have your permission as detailed in the Privacy Policy.

While Users may use the Springer Nature journal content for small scale, personal non-commercial use, it is important to note that Users may not:

1. use such content for the purpose of providing other users with access on a regular or large scale basis or as a means to circumvent access control;
2. use such content where to do so would be considered a criminal or statutory offence in any jurisdiction, or gives rise to civil liability, or is otherwise unlawful;
3. falsely or misleadingly imply or suggest endorsement, approval, sponsorship, or association unless explicitly agreed to by Springer Nature in writing;
4. use bots or other automated methods to access the content or redirect messages
5. override any security feature or exclusionary protocol; or
6. share the content in order to create substitute for Springer Nature products or services or a systematic database of Springer Nature journal content.

In line with the restriction against commercial use, Springer Nature does not permit the creation of a product or service that creates revenue, royalties, rent or income from our content or its inclusion as part of a paid for service or for other commercial gain. Springer Nature journal content cannot be used for inter-library loans and librarians may not upload Springer Nature journal content on a large scale into their, or any other, institutional repository.

These terms of use are reviewed regularly and may be amended at any time. Springer Nature is not obligated to publish any information or content on this website and may remove it or features or functionality at our sole discretion, at any time with or without notice. Springer Nature may revoke this licence to you at any time and remove access to any copies of the Springer Nature journal content which have been saved.

To the fullest extent permitted by law, Springer Nature makes no warranties, representations or guarantees to Users, either express or implied with respect to the Springer nature journal content and all parties disclaim and waive any implied warranties or warranties imposed by law, including merchantability or fitness for any particular purpose.

Please note that these rights do not automatically extend to content, data or other material published by Springer Nature that may be licensed from third parties.

If you would like to use or distribute our Springer Nature journal content to a wider audience or on a regular basis or in any other manner not expressly permitted by these Terms, please contact Springer Nature at

onlineservice@springernature.com